Thin Film Flow Dynamics in Gas-Liquid Contact Reactors

C. Ates, K.V. Muthukumar, M. Okraschevski, N. Bürkle, D.M. Aguirre Bermudez, M. Haber, R. Koch, H.-J. Bauer
Institut für Thermische Strömungsmaschinen (ITS)
Karlsruher Institut für Technologie (KIT)
Karlsruhe, Germany
cihan.ates@kit.edu

***Abstract*—In falling film reactors, the time scale of reaction is typically faster than the time scale of the mass transfer; hence the overall efficiency of the reactor is limited by the rate of mass transport to the reactive interface, which in turn depends on the effective surface area between the liquid phase and the gas phase. Therefore, the performance of these reactors strongly depends on how well the wavy interface dynamics and their influence on the reactive transport are understood at the most fundamental level. In this work, we focused on (i) the creation of a virtual test rig with proper boundary conditions, (ii) the numerical analysis of the wavy interface for alternative liquid distribution strategies with Smoothed Particle Hydrodynamics (SPH) and (iii) how the velocity field in the liquid film changes with oscillating film thickness. In particular, we investigated the flow development in the entry region and how it evolves into a fully developed region for different liquid distribution strategies. We also analyzed the film statistics by extracting the probability density functions of the local film thicknesses in both time and frequency domains. Comparisons between SPH simulations and the available literature confirmed that the deployed numerical solution methodology can capture the global interface dynamics. However, higher residence times must be computed to fully capture the complex local mixing patterns in the fully developed region.**

I. Introduction

The utilization of gas-liquid contact reactors is a popular strategy in the chemical industry for dealing with interfacial transport problems, such as passive cooling systems, gas cleaning units and chemical absorbers. Depending on the physical and chemical properties of the gas and liquid phase, the operating conditions and the reactor configuration, concentration profiles exhibit unique characteristics. For example, when the time scale for diffusion is much longer than the time scale for reaction (i.e., Hatta number (Ha) $>>$ 1), as in the case of CO_2 chemical absorption, all the reactions occur within the film, and the yield is dictated by the effective interfacial area achieved per unit volume. In practice, it is possible to enhance the absorption process by a factor of 20 (on average) for the common CO_2 absorbents if the interface dynamics are properly tuned [1], [2]. Therefore, there lies a great opportunity to improve the reactor performance via engineering the gas-liquid interface, which in turn will smoothen the transition of novel technologies such as CO_2 capture in practice. Realization of this potential, however, requires a thorough understanding of the complex interface dynamics including the transient film thicknesses, velocity distributions and the simultaneous mass transfer process taking place in a very thin concentration boundary layer ($<100\,\mu\mathrm{m}$ [3]).

The utilization of mathematical modeling to identify the coupled mass transfer and flow dynamics at gas-liquid interfaces has received significant attention and has a long history. The vanilla strategy in gas-liquid contact reactor modeling utilizes the enhancement factor (E) models dating back to the early 20th century. Since then, a variety of models have been developed for different gas-liquid mass transfer problems. The dependency of *E* on *Ha* is expressed differently depending on how the mass transfer dynamics are approximated, i.e., by using the film, penetration and surface renewal theories [4]. Unfortunately, such simple models have been shown to fail to reproduce experimental measurements even for integrated (temporally and spatially averaged) CO_2 mass transfer rates for a variety of operating conditions [5]. Another simplifying approach exploited in the last couple of decades is the approximation of film dynamics analytically by combining the diffusion and reaction source terms via linearization or using empirical correlations [6], which also fails to mimic the dynamic nature of the interface [7].

A more comprehensive approach is the use of computational fluid dynamics (CFD) to analyze the mass transfer across the interface, as it has the potential to provide information on the coupled fluid dynamics and reactive transport across the film, which is not easily accessible from the experiments. In fact, the simultaneous solution of the two-phase Navier-Stokes and mass transfer equations is an active research field, yet the progress achieved so far has been limited compared to stand-alone free surface flow problems [8]. The challenges of reactive transport modeling stem from the large jumps in density, species concentration and viscosity across the wavy liquid-gas interface. The corresponding prerequisites of the CFD approach then become (i) accurate and sharp representation of the gas-liquid interface, (ii) ability to capture discontinuities, local penetrations and mixing of the phases, (iii) high temporal and spatial resolutions, (iv) easiness of incorporating chemical kinetics, (v) possibility to trace reaction fronts on top of the

interface tracking and (vi) computational efficiency on parallel architectures.

Lagrangian methods offer an alternative to alleviate these issues, for which the SPH is a strong candidate. Noticeable recent examples with experimental validation related to the modeling of interfaces and wetting phenomena are the uphill movement of a liquid droplet over inclined surfaces [9], droplet wetting behaviour on smooth and rough surfaces [10], flow through porous structures [11], rivulet dynamics on surfaces with different wettabilities [12], flow over micro-structured surfaces [13], droplet flow on inclined structured surfaces [14], the impact of an oblate drop [15], low-speed impact force [16] and fluid-front instabilities in smooth and rough fractures [17]. The capabilities regarding the modeling of wetting phenomena has also been further extended very recently, particularly for the liquid film rupture [18] and superhydrophilic surfaces [19]. With respect to the implementation of the mass transfer and the reaction kinetics, the SPH has been utilized for (i) modeling reactive transport and precipitation in a porous medium (via discretizing the diffusion- reaction equation) [20], [21], (ii) evaluating the concentration field of pollutants in a water tank (only diffusion) [22], (iii) CO_2 sequestration in porous media [23], (iv) multi-component mass transport in the Stefan tube [24], (v) phase separation in ternary mixtures [25], (vi) espresso extraction [26] and (vii) large particle dissolution under flow [27].

In the current work, our focus was mainly set on creating a virtual test rig to analyze the hydrodynamics of the gas-liquid interface, which is the very first step for the dimensioning of the large experimental test rig before its construction. For that purpose, SPH simulations were conducted using alternative liquid distributor designs in large scale reactors to capture the transition from the entry region to the fully developed region for the liquid phase. The results were compared with the available measurements to validate the methodology. Furthermore, practical concerns such as the effect of gas flow rate on the interface dynamics and possible simplifications in the solution domain for higher computational efficiency were discussed.

II. Fundamentals

A. SPH - Schemes

In order to simulate the multiphase flow of air and the liquid film, the SPH method is used to solve the Navier-Stokes equations. The Lagrangian form of the continuity and momentum equation is required to derive the SPH schemes for calculating density ρ, velocity $\vec{v}$, volume forces f, shear stresses τ and static pressure p as a function of space and time t:

$$\frac{D\rho}{Dt} = -\rho\left(\vec{\nabla}\cdot\vec{v}\right), \tag{1}$$

$$\rho\frac{D\vec{v}}{Dt} = -\vec{\nabla}p + \vec{\nabla}\cdot\tau + \rho\vec{f}. \tag{2}$$

In the present study, the mass of each particle is set constant, resulting in inherent mass conservation. A scheme as introduced by Espanol et al. [28] is used to compute the density field. The symmetric scheme is used to discretize the pressure gradient as it conserves linear momentum. Viscous forces are taken into account by following the formulation of Hu and Adam [29]. Following the weakly compressible approach, pressure is determined by means of the Tait equation with additional background pressure to avoid tensile instability [30]. Surface tension is represented by the Continuum Surface Force model [31]. In all cases, particles are flagged by an individual ID numbers which offer the opportunity to track each particle inside the computational domain at each time-step.

III. Computational Setup

The applicability of the outcomes of this work into practice strongly depends on how well the virtual test rig represents the real operating conditions. In accordance, we first looked into the expected film thicknesses as a function of liquid mass flow rate to determine the required spatial (hence temporal) resolution in the SPH domain. The Re number range for water is selected as 10-1000 to ensure a wavy flow regime for water (Kapitza (Ka) number $>$ 3800) [32]. Superficial gas velocity range is set as 1-10 cm/s, following the heuristics for gas-liquid contact reactors. From the available empirical correlations [33], the mean film thickness in the wavy region is found to be around $100\,\mu\mathrm{m}$ to $400\,\mu\mathrm{m}$ (it should be reminded that this value is likely to underestimate the true mean values in flat surfaces). Variations in the measured film thicknesses in time for similar flow conditions [34] further indicated that the instantaneous film thickness could be couple of times larger than the mean value; hence instantaneous film thicknesses are expected to be between $100-1000\,\mu\mathrm{m}$. Based on these heuristics, a mean liquid inlet velocity of 10 cm/s with an initial film thickness of 1 mm is set at the inlet boundary. Gas velocity was changed between 1 cm/s to 50 cm/s for alternative scenarios. In order to balance the requirements for high spatial resolution and the long simulation times, a spatial resolution of $50\,\mu\mathrm{m}$ was selected.

The exact wave characteristics cannot be known a priori; therefore, it is difficult to define the height of the virtual reactor to capture these wave dynamics. Nonetheless, as the wavelengths are expected to be less than 10 cm in Re =100-1000, we started with an effective reactor height of 20 cm, which was later extended to 1 m. Since the three-dimensional waves are chaotic in nature, we started with 2D systems to capture an ordered behavior, which is the very first step towards understanding the hydrodynamics of the wavy film flows. We were also able to use the available experimental and theoretical studies that were conducted with 2D wavy flows as an approximate benchmark for this very first configuration. With respect to the liquid distributors, we have tested three configurations shown in Figure 1 as a starting point. In Case A, we assume to deploy a narrow-slit type distributor through which the solvent is fed. In Case B and C, we tested the effect of “film conditioning” on the evolution of the thin film flow.

We also tested two limiting gas velocities for Case C in order to explore the effect of counter-current flowing gas velocities on the interface dynamics.

All simulations were conducted with a temporal resolution

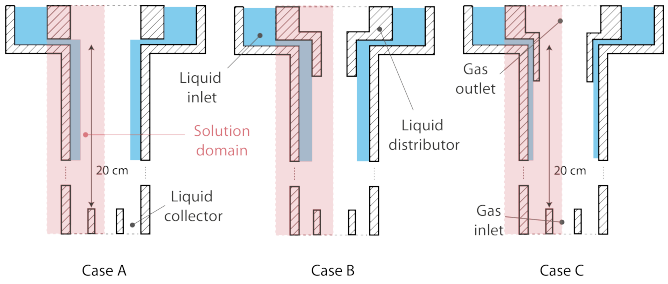

Fig. 1. 2D reactors implemented in the SPH domain with alternative liquid distributors

of 14 MHz ($\Delta t \sim 70\,\mathrm{ns}$), while the quantities of interest (positions, velocity components, pressure, density, fluid type, and unique particle IDs) were exported with a frequency of 250 Hz. This voluminous data is then post-processed to extract the local film thicknesses and velocity components at every stored time step. Data extraction is done by mounting "virtual probes" along the reactor at 2 cm intervals, which record both the film thicknesses and velocity components.

IV. Results and Discussions

A. Analysis of the Developing Gas-Liquid Interface

Our objectives in these virtual tests were (i) to investigate the transient nature of the wavy interface, (ii) to determine the time required for steady conditions, (iii) to find the height required to reach developed flow, and finally (iv) assess the effect of liquid distribution on the developing wavy interface.

The analysis of the development of the local film thicknesses

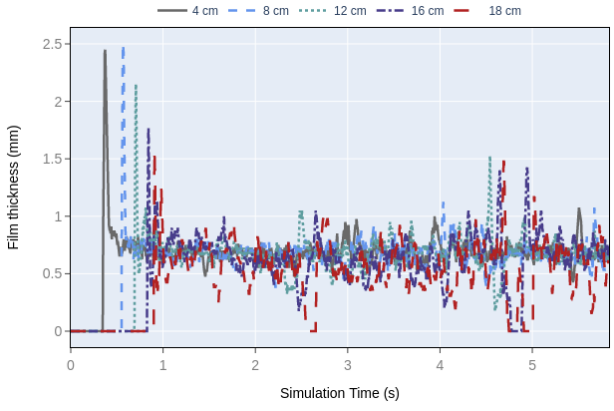

Fig. 2. Temporal variations in falling film thicknesses for base geometry (Case A).

revealed that it takes about 1 second to wet the reactor surface, where the initial wetting can be detected as a sudden increase in the film thickness (Figure 2). After the wetting, an oscillatory behavior was observed, which grows downstream of the liquid inlet. It is also seen that there are some brief periods of time where the film thickness drops to zero (e.g., t=2.7 s at 18 cm), indicating a partial wetting which is not desired. After reaching relatively steady conditions (t>3 s), film thickness still exhibits large local oscillations, as expected in the wavy region. These oscillations were also found to be growing downstream, while the mean film thickness decreases as the film flows. At the exit, the average film thickness was found to be around 0.52 mm.

We further looked into the film statistics by extracting the

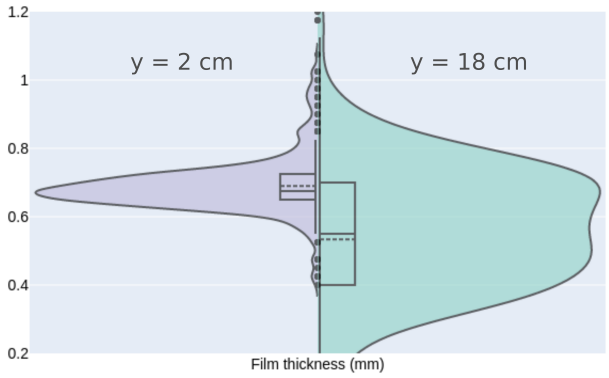

Fig. 3. PDF of film thicknesses at different locations (statistics are derived for 3-6 seconds). y axis is in the direction of gravity

probability density functions (PDF) of the local film thicknesses (Figure 3). Close to the liquid distributor (2 cm), the PDF has symmetric variation around a mean value (horizontal line in the box plot), yet we still observe the nucleation of larger waves, resulting in small hills at the higher end of the PDF. Herein, the largest peak can be considered as the film substrate thickness, while the width of the PDF is a measure of the wave amplitude. As we go downstream of the reactor (Figure 3, y=18 cm), the width of the PDF broadens, i.e.,

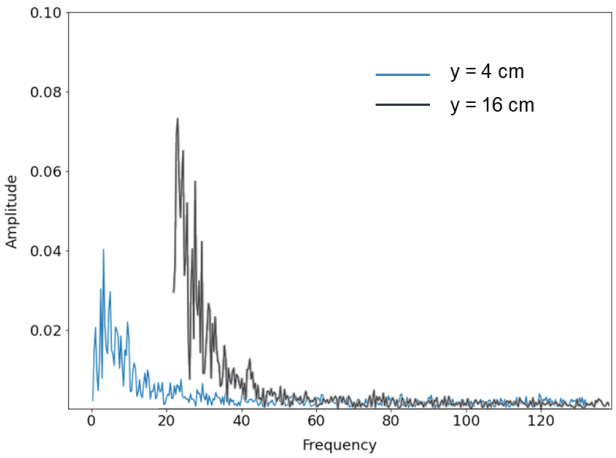

Fig. 4. Power spectrum density for the film thicknesses at 4 and 16 cm downstream the reactor inlet (Case A). Film thickness information is recorded between 3-6 seconds. The signal at 16 cm is shifted in the frequency axis for a better visibility.

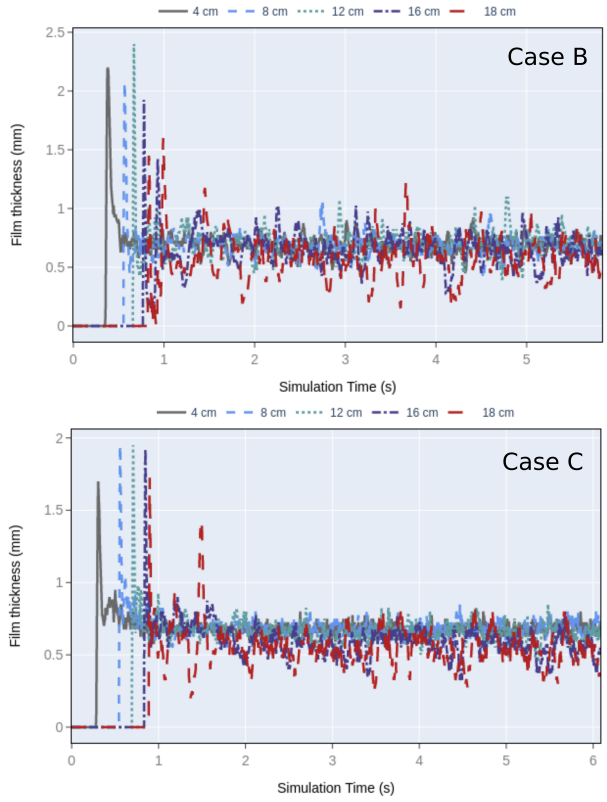

Fig. 5. Temporal variations in the falling film thicknesses for Case B and C along the reactor.

wave amplitudes increase. There also appear additional peaks at both ends, corresponding to other small and large amplitude waves. Towards the exit of the reactor, the mean film thickness is lowest, fluctuating due to the presence of multiple waves.
The hypothesis of multi-wave flow can be tested by transforming the wave signals into the frequency domain via Fast Fourier Transform (FFT), as shown in Figure 4. It is clearly seen that multiple large amplitude waves evolve at low frequencies along the reactor, which in turn leads to the flatter PDFs in the film thicknesses (Figure 3).

B. Influence of Liquid Distributors

In the next step, we changed the design of the liquid distributor and proposed two alternative modifications (Figure 1) to overcome the growing instabilities, hence the partial surface wetting. Variations in the film thicknesses under the same operating conditions are illustrated in Figure 5. Similar to Case A, the reactor walls were completely wetted within the first second. With the flow conditioning, however, flow stability has been increased noticeably, and the partial wetting problem in later times was alleviated completely. At a closer look, fluctuations of film thickness at y=16 cm and 18 cm were even getting closer (i.e., converged) when we forced the film to flow through a gap of 0.5 mm (Case C). For both Case B and C, the deviations in the film thicknesses were also much smaller compared to Case A. In other words, with proper guidance of the downstream flow, it may be possible to reach the developed conditions at smaller residence times (hence reactor volumes).
Improvement in the flow characteristics was even more striking when we examined the flow statistics (Figure 6). When Case A and B are compared, it is seen that additional waves reflected as small hills at the upper end of the PDF at 2 cm are suppressed. More importantly, the flat PDF profile (Case A at 18 cm) is replaced by a curve, indicating a more dominant, single wave.
Wave statistics along the reactor walls are illustrated as ridgeline plots (Figure 6, right), which further highlights the suppression of the growing instability. When the liquid inlet is further conditioned with a narrower exit gap (Case C: gap width is set to expected averaged film thickness), the impact of the liquid distributor can be seen even very close to the inlet (at 2 cm), where the film thickness was forced to be narrower (0.5 mm, compared to the previous gap of 1 mm). Herein, the PDF function takes a much narrower distribution. Moreover, the fluctuations in the film thickness were more symmetric and had a smaller variance.
The effect of the liquid distributor on wave dynamics is also visible in the frequency domain. PSD signals (Figure 7) reveal that the amplitude of the large peaks corresponding to the rolling waves gets smaller and more stable for Case B and C, whereas the width of the large-signal gets even narrower for Case C. A cascade of capillary waves is visible in all cases, as expected.

C. Effect of Gas Flow Rate on the interface

The possible effect of counter-current gas flow rate on the film dynamics was analyzed for Case C, where the free stream gas velocities were reduced to 1 cm/s from 50 cm/s (base gas velocity). The comparisons revealed that gas velocity had only a minor effect on the mean film thicknesses in this flow regime but demonstrated a more profound impact on the PDFs. Nonetheless, the overall behavior of the interface remained similar in both cases. This similarity indicates the possibility of utilizing single-phase, free-surface flows as an approximation for the parametric analysis of the film flow dynamics, which would, in turn, decrease the total number of simulated SPH particles.

D. Discussions

In the current work, we created a virtual test rig in the SPH domain to analyze the thin film flow dynamics. For this purpose, we identified the representative flow regimes and set the initial and boundary conditions to mimic the gas-liquid contact reactor applications in the wavy operational regime. We also proposed and tested alternative liquid distributor options to identify the impact of film conditioning on the film thickness statistics. An overall comparison of our predictions (Case C) with the available literature is shown in Figure 9. By selecting proper boundary conditions, we could be able to generate the same global behavior with the measured values

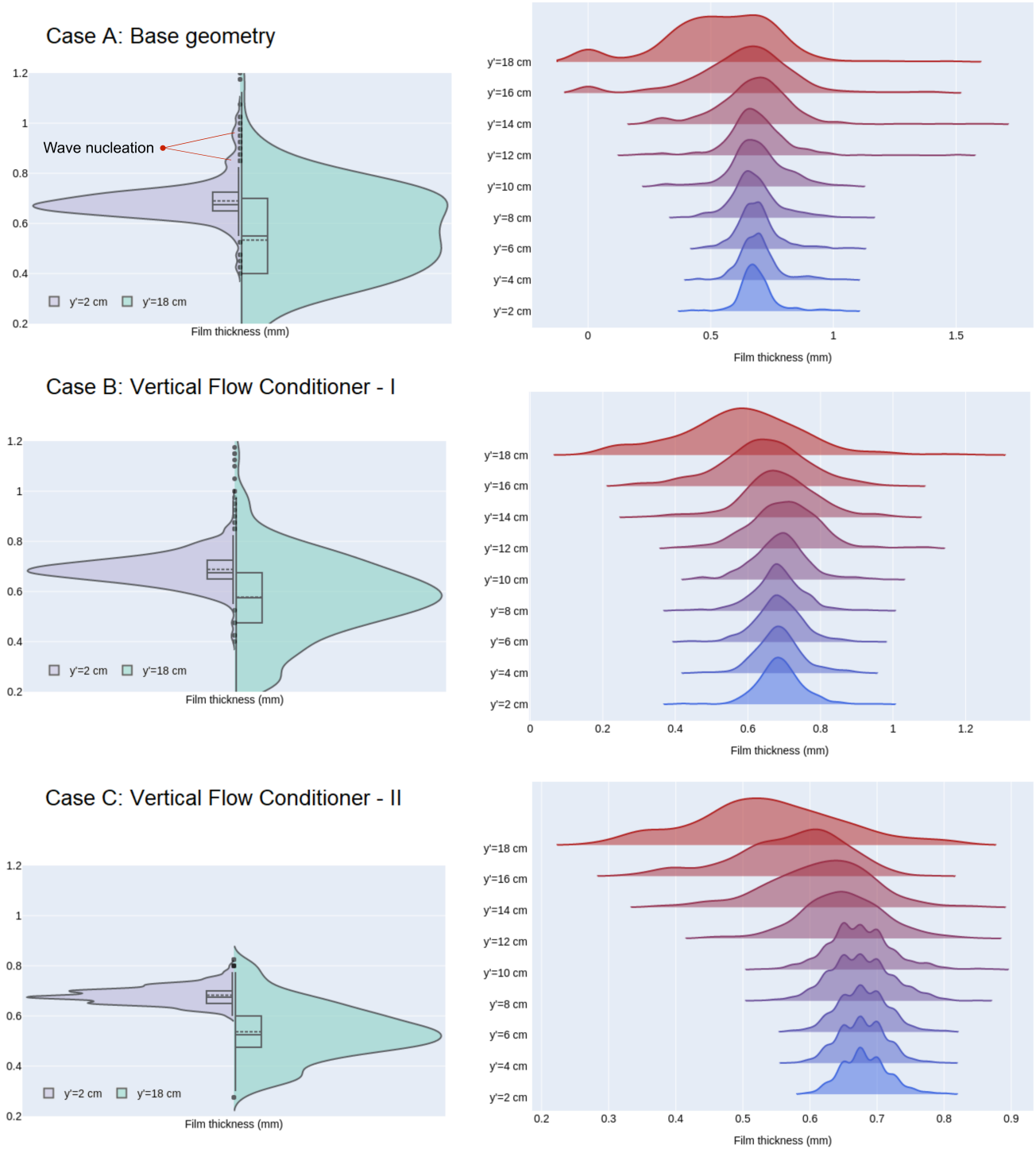

Fig. 6. PDFs for film thickness variations between 2 cm and 18 cm downstream of the liquid inlet for three liquid distributor designs. Left: PDF functions, Right: Ridgeline plots showing the evolution of PDFs along the reactor. (statistics are derived for 3-6 seconds; u_{gas}=50 cm/s)

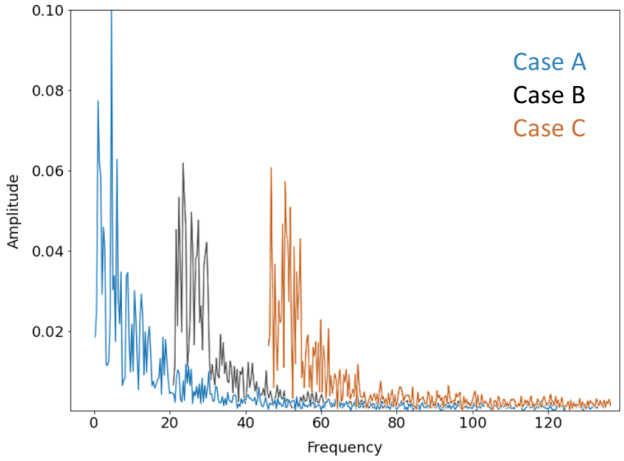

Fig. 7. Comparison of PSDs for Case A, B and C. FFT is performed on film thickness profiles calculated between 3-6 s, 18 cm downstream of the liquid inlet. The signals for Case B and C are shifted in frequency axis for a better visibility.

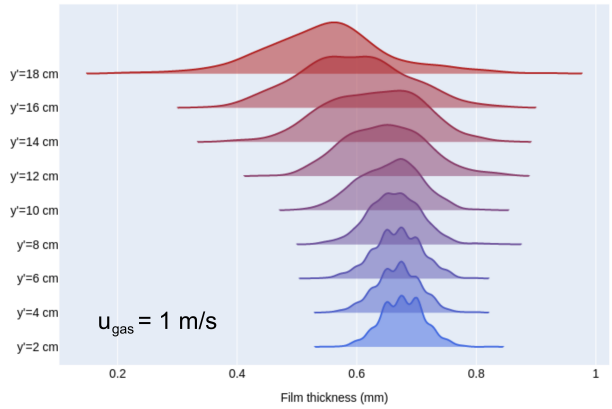

Fig. 8. Effect of the superficial gas velocity on the film thickness: low gas velocity, Case C.

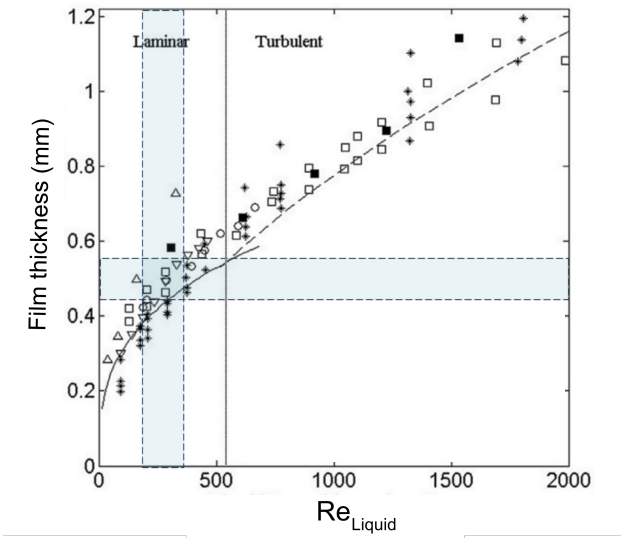

Fig. 9. Mean film thickness measurements over a wide range of Re. Re for the gas phase is zero [35]. SPH simulation results for Case 3 (t > 3s) are highlighted with light blue boxes.

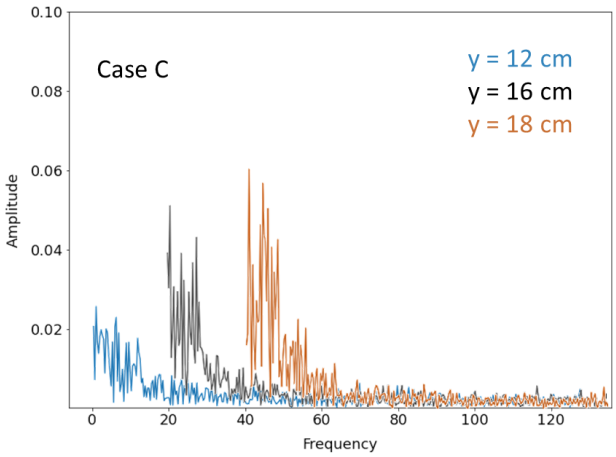

Fig. 10. Power spectrum density for the film thicknesses at various locations (Case C). Film thickness information is recorded between 3-6 s.

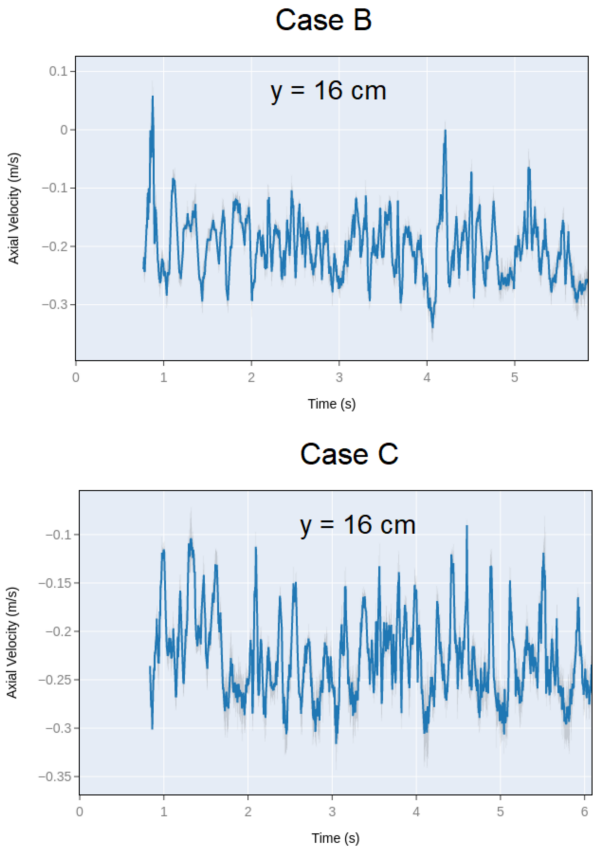

Fig. 11. Temporal fluctuations in mean axial velocities at y = 16 cm for Case B and C.

under the same liquid mass flow rates, which proves the capabilities of the deployed modeling strategy for the thin film flow problem.

It should be highlighted that we had selected a reactor height of 20 cm ($= 200 \times d_{film}$) as an "educated guess" and analyzed the results to see whether we had reached the fully developed

region or not. With the help of the FFT analysis (Figure 10), it is revealed that the film flow has indeed started to converge, yet 20 cm height is not sufficient to capture the developed region. Herein, the simulated film flow might also be suffering from the exit boundary effects, which may be the reason for the second peak in PDF tails observed in Figure 6 towards the exit of the reactor. In other words, there is a need for extending the simulated reactor height at least a couple of times to be sure of capturing the transition to the wavy developed flow. It also means that we need to extend the simulation time a couple of more times to match the changing residence times. Another issue is the spatial resolution of the solution domain, which is currently $50\,\mu\mathrm{m}$. It means that we have only about ten particles in the lateral direction when the film is thin, which is insufficient to capture the internal mixing in the liquid phase. Temporal fluctuations in the mean axial velocity component are shown in Figure 11 for Case B and C. Although we captured a noticeable variation, the spatial resolution has to be increased to track the micro-mixing in the liquid film. Both issues are currently being addressed in a follow-up study.

V. Conclusion

- A virtual test rig in the SPH domain has been tailored for the gravity-driven thin film flow reactor under realistic flow conditions.
- Our methodology has been confirmed by benchmarking the SPH predictions with those of theory and available experimental measurements.
- Conditioning the flow with a distributor plate increased the flow stability and alleviated the partial wetting problem. Herein, heuristic correlations can be utilized to as an initial guess for the gap width.
- The simulated height (20 cm) was not sufficient to capture the complete transition to the developed regime. It is also seen that higher spatial resolutions ($< 50\,\mu\mathrm{m}$) are required to better capture the micro-mixing phenomena within the film.

Acknowledgment

This work was performed on the HoreKa supercomputer funded by the Ministry of Science, Research and the Arts Baden-Württemberg and by the Federal Ministry of Education and Research. The study is financially supported by the Friedrich and Elisabeth Boysen Foundation.

References

[1] D. W. Green and R. H. Perry, *Perry's Chemical Engineers' Handbook, Eighth Edition*, 8th ed. New York: McGraw-Hill Education, 2008.

[2] P. N. Yoshimura, T. Nosoko, and T. Nagata, "Enhancement of mass transfer into a falling laminar liquid film by two-dimensional surface waves-some experimental observations and modeling," *Chemical Engineering Science*, vol. 51, no. 8, pp. 1231–1240, 1996.

[3] J. Hu, X. Yang, J. Yu, and G. Dai, "Numerical simulation of carbon dioxide (CO2) absorption and interfacial mass transfer across vertically wavy falling film," *Chemical Engineering Science*, vol. 116, pp. 243–253, 2014. [Online]. Available: http://dx.doi.org/10.1016/j.ces.2014.05.002

[4] L. K. Doraiswamy and D. Uner, *Chemical reaction engineering : beyond the fundamentals*, 1st ed. New York: Taylor Francis, 2014.

[5] K. R. Putta, F. A. Tobiesen, H. F. Svendsen, and H. K. Knuutila, "Applicability of enhancement factor models for CO2 absorption into aqueous MEA solutions," *Applied Energy*, vol. 206, no. February, pp. 765–783, 2017. [Online]. Available: https://doi.org/10.1016/j.apenergy.2017.08.173

[6] G. Zahedi, A. Jahanmiri, A. Elkamel, and A. Lohi, "Mathematical modeling, simulation, and experimental verification of CO2 removal in a turbulent contact absorber," *Chemical Engineering and Technology*, vol. 29, no. 8, pp. 916–922, 2006.

[7] S. Norouzbahari, S. Shahhosseini, and A. Ghaemi, "CO2 chemical absorption into aqueous solutions of piperazine: Modeling of kinetics and mass transfer rate," *Journal of Natural Gas Science and Engineering*, vol. 26, pp. 1059–1067, 2015. [Online]. Available: http://dx.doi.org/10.1016/j.jngse.2015.07.048

[8] P. Bandi, M. Modigell, S. Groß, A. Reusken, L. Zhang, Y. Heng, W. Marquardt, and A. Mhamdi, "On reduced modeling of mass transport in wavy falling films," *AIChE Journal*, vol. 64, no. 6, pp. 2265–2276, 2018.

[9] A. K. Das and P. K. Das, "Multimode dynamics of a liquid drop over an inclined surface with a wettability gradient," *Langmuir*, vol. 26, no. 12, pp. 9547–9555, 2010.

[10] J. Kordilla, A. M. Tartakovsky, and T. Geyer, "A smoothed particle hydrodynamics model for droplet and film flow on smooth and rough fracture surfaces," *Advances in Water Resources*, vol. 59, pp. 1–14, 2013. [Online]. Available: http://dx.doi.org/10.1016/j.advwatres.2013.04.009

[11] A. M. Aly and M. Asai, "Three-Dimensional Incompressible Smoothed Particle Hydrodynamics for Simulating Fluid Flows Through Porous Structures," *Transport in Porous Media*, vol. 110, no. 3, pp. 483–502, 2015.

[12] S. Moghtadernejad, M. Jadidi, A. Dolatabadi, and N. Esmail, "SPH Simulation of Rivulet Dynamics on Surfaces with Various Wettabilities," *SAE International Journal of Aerospace*, vol. 8, no. 1, pp. 160–173, 2015.

[13] L. Lin, R. Sampath, N. T. Dinh, and N. Akinci, "A computational study of thin film dynamics on micro-structured surfaces," *ASME 2016 Heat Transfer Summer Conference, HT 2016, collocated with the ASME 2016 Fluids Engineering Division Summer Meeting and the ASME 2016 14th International Conference on Nanochannels, Microchannels, and Minichannels*, vol. 2, no. June, 2016.

[14] E. Shigorina, A. M. Tartakovsky, and J. Kordilla, "Investigation of Gravity-Driven Infiltration Instabilities in Smooth and Rough Fractures Using a Pairwise-Force Smoothed Particle Hydrodynamics Model," *Vadose Zone Journal*, vol. 18, no. 1, pp. 1–12, 2019.

[15] X. Yang and S. C. Kong, "3D Simulation of Drop Impact on Dry Surface Using SPH Method," *International Journal of Computational Methods*, vol. 15, no. 3, pp. 1–23, 2018.

[16] R. Zhang, B. Zhang, Q. Lv, J. Li, and P. Guo, "Effects of droplet shape on impact force of low-speed droplets colliding with solid surface," *Experiments in Fluids*, vol. 60, no. 4, pp. 1–13, 2019. [Online]. Available: http://dx.doi.org/10.1007/s00348-019-2712-7

[17] E. Shigorina, A. M. Tartakovsky, and J. Kordilla, "Investigation of Gravity-Driven Infiltration Instabilities in Smooth and Rough Fractures Using a Pairwise-Force Smoothed Particle Hydrodynamics Model," *Vadose Zone Journal*, vol. 18, no. 1, pp. 1–12, 2019.

[18] X. Xu, M. Dey, M. Qiu, and J. J. Feng, "Modeling of van der Waals force with smoothed particle hydrodynamics: Application to the rupture of thin liquid films," *Applied Mathematical Modelling*, vol. 83, pp. 719–735, 2020. [Online]. Available: https://doi.org/10.1016/j.apm.2020.03.003

[19] M. Olejnik and J. Pozorski, "A Robust Method for Wetting Phenomena Within Smoothed Particle Hydrodynamics," *Flow, Turbulence and Combustion*, vol. 104, no. 1, pp. 115–137, 2020.

[20] P. Meakin and A. M. Tartakovsky, "Modeling and Simulation of Pore-Scale Multiphase Fluid Flow and Reactive," *Transport*, vol. 47, no. 2008, pp. 1–47, 2009. [Online]. Available: http://www.agu.org/pubs/crossref/2009/2008RG000263.shtml

[21] A. M. Tartakovsky, N. Trask, K. Pan, B. Jones, W. Pan, and J. R. Williams, "Smoothed particle hydrodynamics and its applications for multiphase flow and reactive transport in porous media," *Computational Geosciences*, vol. 20, no. 4, pp. 807–834, 2016.

[22] F. Aristodemo, I. Federico, P. Veltri, and A. Panizzo, "Two-phase SPH modelling of advective diffusion processes," *Environmental Fluid Mechanics*, vol. 10, no. 4, pp. 451–470, 2010.

[23] U. C. Bandara, B. J. Palmer, and A. M. Tartakovsky, "Effect of wettability alteration on long-term behavior of fluids in subsurface," *Computational Particle Mechanics*, vol. 3, no. 2, pp. 277–289, 2016.
[24] M. Hirschler, W. Säckel, and U. Nieken, "On Maxwell–Stefan diffusion in Smoothed Particle Hydrodynamics," *International Journal of Heat and Mass Transfer*, vol. 103, pp. 548–554, 2016. [Online]. Available: http://dx.doi.org/10.1016/j.ijheatmasstransfer.2016.07.061
[25] M. Hopp-Hirschler, J. Baz, N. Hansen, and U. Nieken, "Generalized Fickian approach for phase separating fluid mixtures in Smoothed Particle Hydrodynamics," *Computers and Fluids*, vol. 179, pp. 78–90, 2019. [Online]. Available: https://doi.org/10.1016/j.compfluid.2018.10.020
[26] M. Ellero and L. Navarini, "Mesoscopic modelling and simulation of espresso coffee extraction," *Journal of Food Engineering*, vol. 263, no. December 2018, pp. 181–194, 2019. [Online]. Available: https://doi.org/10.1016/j.jfoodeng.2019.05.038
[27] A. Rahmat, M. Barigou, and A. Alexiadis, "Numerical simulation of dissolution of solid particles in fluid flow using the SPH method," *International Journal of Numerical Methods for Heat and Fluid Flow*, vol. 30, no. 1, pp. 290–307, 2019.
[28] P. Español and M. Revenga, "Smoothed dissipative particle dynamics," *Phys. Rev. E*, vol. 67, p. 026705, Feb 2003.
[29] X. Y. Hu and N. A. Adams, "Angular-momentum conservative smoothed particle dynamics for incompressible viscous flows," *Physics of Fluids*, vol. 18, no. 10, p. 101702, 2006.
[30] M. B. Liu and G. R. Liu, "Smoothed particle hydrodynamics (sph): an overview and recent developments," *Archives of Computational Methods in Engineering*, vol. 17, no. 1, pp. 25–76, 2010.
[31] S. Adami, X. Y. Hu, and N. A. Adams, "A new surface-tension formulation for multi-phase {SPH} using a reproducing divergence approximation," *Journal of Computational Physics*, vol. 229, no. 13, pp. 5011 – 5021, 2010.
[32] A. Åkesjö, M. Gourdon, L. Vamling, F. Innings, and S. Sasic, "Hydrodynamics of vertical falling films in a large-scale pilot unit – a combined experimental and numerical study," *International Journal of Multiphase Flow*, vol. 95, pp. 188–198, 2017. [Online]. Available: https://www.sciencedirect.com/science/article/pii/S0301932216307789
[33] K. Moran, J. Inumaru, and M. Kawaji, "Instantaneous hydrodynamics of a laminar wavy liquid film," *International Journal of Multiphase Flow*, vol. 28, no. 5, pp. 731–755, 2002. [Online]. Available: https://www.sciencedirect.com/science/article/pii/S030193220200006X
[34] Y. Yu, S. Wei, Y. Yang, and X. Cheng, "Experimental study of water film falling and spreading on a large vertical plate," *Progress in Nuclear Energy*, vol. 54, no. 1, pp. 22–28, 2012. [Online]. Available: https://www.sciencedirect.com/science/article/pii/S0149197011001892
[35] I. Zadrazil, O. K. Matar, and C. N. Markides, "An experimental characterization of downwards gas-liquid annular flow by laser-induced fluorescence: Flow regimes and film statistics," *International Journal of Multiphase Flow*, vol. 60, pp. 87–102, 2014. [Online]. Available: http://dx.doi.org/10.1016/j.ijmultiphaseflow.2013.11.008